Journal of Nuclear Medicine, published on November 13, 2014 as doi:10.2967/jnumed.114.145151

First-in-Human Evaluation of ^{18}F-Mefway, a PET Radioligand Specific to Serotonin-1A Receptors

Ansel T. Hillmer[1,2], Dustin W. Wooten[1,2], Alisha K. Bajwa[3], Andrew T. Higgins[2], Patrick J. Lao[1,2], Tobey J. Betthauser[1,2], Todd E. Barnhart[1], Howard A. Rowley[4], Charles K. Stone[5], Sterling C. Johnson[6], Jogeshwar Mukherjee[3], and Bradley T. Christian[1,2,7]

[1]Department of Medical Physics, University of Wisconsin, Madison, Wisconsin; [2]Waisman Center for Brain Imaging and Behavior, University of Wisconsin, Madison, Wisconsin; [3]Department of Radiological Sciences, University of California, Irvine, California; [4]Department of Radiology, University of Wisconsin, Madison, Wisconsin; [5]Department of Medicine, University of Wisconsin, Madison, Wisconsin; [6]Department of Geriatrics, University of Wisconsin, Madison, Wisconsin; and [7]Department of Psychiatry, University of Wisconsin, Madison, Wisconsin

The serotonin-1A (5-HT$_{1A}$; 5-HT is 5-hydroxytryptamine) receptor is implicated in an array of neurologic and psychiatric disorders. Current PET radioligands targeting 5-HT$_{1A}$ receptors have limitations hindering widespread PET studies of this receptor system. The 5-HT$_{1A}$–specific antagonist radioligand *N*-{2-[4-(2-methoxyphenyl) piperazinyl]ethyl}-*N*-(2-pyridyl)-*N*-(*trans*-4-^{18}F-fluoromethylcyclohexane) carboxamide (^{18}F-mefway) exhibited promising in vivo properties in rhesus monkeys. The goal of this work was to examine the in vivo cerebral binding profile and metabolism of ^{18}F-mefway in humans. **Methods:** Dynamic ^{18}F-mefway PET data were acquired for 6 healthy volunteers (4 women, 2 men; age, 22–38 y). Scans were initiated with the injection of 192–204 MBq of radiotracer, and data were acquired for 2 h. Venous blood samples were collected and assayed to examine the in vivo metabolism profile of ^{18}F-mefway. To examine the test–retest variability of ^{18}F-mefway, a second PET scan was acquired at least 2 wk later for 4 subjects. Regional binding potentials (BP_{ND}s) were calculated with the multilinear reference tissue model, and voxelwise BP_{ND} maps were calculated with Logan graphical analysis. Regions surrounding the brain were carefully inspected for uptake of radiolabeled species in bone. **Results:** ^{18}F-mefway uptake in the brain occurred quickly, with a peak standardized uptake value (SUV) of 1.7. Rapid washout in the cerebellum resulted in SUVs of 0.2 at 120 min, whereas regions with specific 5-HT$_{1A}$ binding exhibited retention of radioligand, yielding SUVs of 0.4–0.9 at 120 min. Rapid metabolism of ^{18}F-mefway was observed, with no detected ^{18}F-fluoride ions in plasma. BP_{ND} values of 2.4 were measured in the mesial temporal lobe, with values of 1.6 in the insular cortex and 0.7–1.0 in other cortical regions. Stable BP_{ND} estimates were obtained using 90 min of dynamic data. Average test–retest variability was 8%. No evidence of radioactivity uptake in bone was observed. **Conclusion:** ^{18}F-mefway exhibits favorable in vivo properties for serotonin 5-HT$_{1A}$ receptor measurements in humans. The simple radiosynthesis, high specific binding profile, and absence of PET signal in bone make ^{18}F-mefway an attractive radiotracer for PET experiments examining the 5-HT$_{1A}$ receptor in neuropsychiatric disorders and drug intervention.

Key Words: PET; ^{18}F-mefway; serotonin-1A; hippocampus

J Nucl Med 2014; 55:1–7
DOI: 10.2967/jnumed.114.145151

The neurotransmitter 5-hydroxytryptamine (5-HT; serotonin) is a crucial regulator of many cognitive processes including memory, learning, and mood. The 5-HT$_{1A}$ receptor is a G-protein–coupled receptor that plays a vital role in regulating 5-HT transmission. These receptors occur presynaptically as autoreceptors in the raphe nuclei (*1*) and postsynaptically in cortical and hippocampal regions (*2*). Brain regions rich in 5-HT$_{1A}$ receptor concentrations include the mesial temporal lobe (MTL), cingulate cortex, raphe nuclei, frontal cortex, and parietal cortex. The 5-HT$_{1A}$ receptor is implicated in a variety of neuropsychiatric pathologies, including schizophrenia, Alzheimer disease, depressive disorders, and alcohol dependence.

An important experimental technique for in vivo interrogation of 5-HT$_{1A}$ receptors is PET imaging. To date, the most commonly used PET antagonist radioligand for 5-HT$_{1A}$ receptors is ^{11}C-WAY-100635 (*3*). This radioligand exhibits high signal in regions of specific binding relative to the cerebellum and suitable regional binding potential (BP_{ND}) quantification; however, widespread use of this radioligand has been limited. The radiochemical production for ^{11}C-WAY-100635 is difficult to reliably perform, and the short 20-min half-life of the ^{11}C label requires an on-site cyclotron and yields poor counting statistics toward the end of scanning procedures. To overcome these issues, a variety of WAY-100635 analogs with the longer-lived ^{18}F label (110-min half-life) have been developed (*4*). 2′-methoxyphenyl-(*N*-2′-pyridinyl)-*p*-^{18}F-fluorobenzamidoethylpiperazine (^{18}F-MPPF) has been successfully used to study 5-HT$_{1A}$ physiology in human subjects but suffers from poor brain penetration and subsequently yields low target-to-background ratios (*5*). ^{18}F-FCWAY has kinetic properties similar to ^{11}C-WAY-100635 and a simple labeling procedure (*6*). However, defluorination of ^{18}F-FCWAY in vivo resulted in bone uptake of ^{18}F-fluoride ions, complicating analysis of PET data (*7*) and requiring enzyme inhibitors to enable suitable quantification (*8*).

The radioligand *N*-{2-[4-(2-methoxyphenyl)piperazinyl]ethyl}-*N*-(2-pyridyl)-*N*-(4-^{18}F-fluoromethylcyclohexane)carboxamide was

Received Jul. 7, 2014; revision accepted Sep. 30, 2014.
For correspondence or reprints contact: Bradley T. Christian, 1500 Highland Ave., Madison, WI 53705.
E-mail: bchristian@wisc.edu
Published online ••••••••••••.

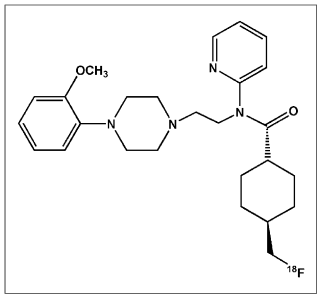

FIGURE 1. Chemical structure of *trans*-^{18}F-mefway.

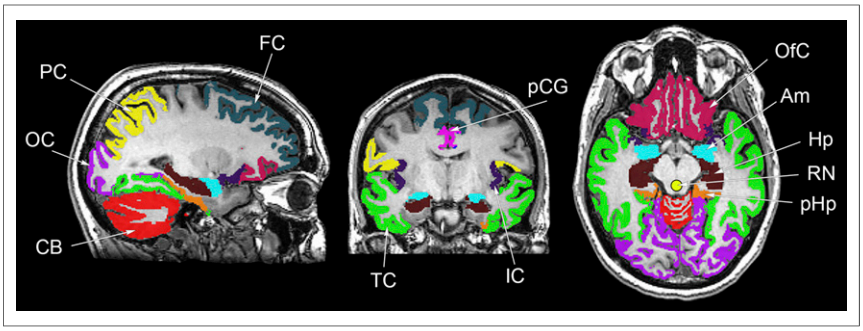

RGB

FIGURE 2. Regions used for analysis of ^{18}F-mefway PET data. Regions defined by template-based FreeSurfer algorithm included amygdala (Am), hippocampus (Hp), parahippocampal gyrus (pHp), insular cortex (IC), anterior cingulate gyrus (aCG; not shown), posterior cingulate gyrus (pCG), parietal cortex (PC), orbitofrontal cortex (OfC), temporal cortex (TC), occipital cortex (OC), frontal cortex (FC), and cerebellum (CB). Hand-drawn raphe nuclei (RN) is also shown.

designed to provide an ^{18}F-labeled analog of ^{11}C-WAY-100635 with improved stability by moving the radiolabel from an aromatic ring to a primary carbon. Studies of the *cis* and *trans* isomers of this radioligand revealed high specificity of the *trans* isomer for 5-HT$_{1A}$ receptors (*9*); therefore, this human study focused on the [Fig. 1] *trans* isomer, shown in Figure 1 (henceforth abbreviated as ^{18}F-mefway). ^{18}F-mefway is produced with high yields (*10*), and preclinical experiments demonstrated comparable kinetic properties between ^{11}C-WAY-100635 and ^{18}F-mefway in rhesus monkeys with no evidence of defluorination (*11*).

Studies investigating 5-HT$_{1A}$ receptor physiology in nonhuman primates using ^{18}F-mefway have also been performed in our laboratories. These findings include sex-based differences in 5-HT$_{1A}$ function, for which increased in vivo affinity of ^{18}F-mefway for the 5-HT$_{1A}$ receptor and decreased 5-HT$_{1A}$ binding potentials in women relative to men were observed (*12*). Additionally, decreased 5-HT$_{1A}$ binding levels in 5-HTTLPR *s*-carriers (*13*) and increased 5-HT$_{1A}$ binding levels after chronic alcohol self-administration have been reported (*14*). These ^{18}F-mefway studies therefore indicated great promise of a suitable ^{18}F-labeled radioligand to image 5-HT$_{1A}$–specific physiology in humans.

The goal of this work was to evaluate the in vivo properties of ^{18}F-mefway in humans for the first time. The regional distribution of ^{18}F-mefway uptake and binding in the human brain is reported, including a detailed inspection of ^{18}F-mefway binding in the MTL, an important region with high 5-HT$_{1A}$ density. Furthermore, a preliminary analysis of ^{18}F-mefway's behavior in venous plasma samples is performed.

MATERIALS AND METHODS

Subjects

Subjects were healthy volunteers consisting of 4 women and 2 men, ranging in age from 22 to 38 y, recruited at the University of Wisconsin–Madison. The University of Wisconsin Institutional Review Board approved all study procedures. All subjects provided informed signed consent forms before participation. Antidepressive medication was verbally screened for as an exclusion criterion.

Scanning Procedures

^{18}F-mefway was produced following previously published methods (*9*). The synthesis consisted of a nucleophilic substitution of the precursor, *N*-{2-[4-(2-methoxyphenyl)piperazinyl]ethyl}-*N*-(2-pyridyl)-*N*-(*trans*-4-tosyloxymethylcyclohexane)carboxamide (*tosyl-trans*-mefway; Huayi Isotopes), with cyclotron-produced ^{18}F-fluoride ions at 96°C to synthesize ^{18}F-mefway. Reversed-phase C18 high-performance liquid chromatography purification with a mobile phase of 50:50:0.1 MeCN:H_2O:triethylamine was then performed. Solvents were removed via C18 sep-pak extraction. The final product was formulated in 9 mL of sterile saline and 1 mL of EtOH and filter-sterilized.

^{18}F-mefway PET data were acquired on an EXACT HR+ PET scanner (Siemens) using 3-dimensional mode. A 6-min transmission scan using ^{68}Ge rod sources was first acquired for attenuation correction. Dynamic PET data acquisition was initiated with a bolus injection of 192–204 MBq of ^{18}F-mefway, and data were acquired for 120 min. Venous samples of 1.0 mL were acquired from the cephalic vein (opposite the injection arm) approximately 5, 15, 30, 60, 90, and 120 min after injection. At least 2 wk after the first scan, 5 of the 6 subjects returned for a second ^{18}F-mefway scanning procedure to assess the test–retest reproducibility of ^{18}F-mefway imaging. The mean and SD of the administered mass of ^{18}F-mefway was 56 ± 50 ng (range, 12–143 ng). The mean administered activity of ^{18}F-mefway was 199 ± 4 MBq (range, 192–204 MBq). There were no adverse or clinically detectable pharmacologic effects, including no significant changes to vital signs or laboratory results, in any of the 6 subjects.

MR imaging data were acquired on a 3.0-T MR750 scanner (GE Healthcare) with an 8-channel head coil. A T1-weighted Spoiled Gradient REcalled Acquisition volume was acquired using the following parameters: inversion time/echo time/repetition time, 450/3.2/8.2 ms; flip angle, 12°; slice thickness, 1 mm no gap; field of view, 256; and matrix size, 256 × 256.

Data Processing and Analysis

Venous blood samples were analyzed to assay ^{18}F-mefway metabolism in vivo. Samples of 1.0 mL of whole blood mixed with 50 μL of heparinized saline were centrifuged for 5 min. Next, 0.5 mL of plasma was extracted and mixed with 50 μL of 5.5% sodium bicarbonate and 0.5 mL of acetonitrile, followed by vigorous mixing to denature the proteins. After the protein precipitate settled, 0.5 mL of liquid was extracted, concentrated, and spotted on an alumina thin-layer chromatography (TLC) plate (Whatman). The TLC plate was developed in a mobile phase of 50:50 MeOH:10% ammonium acetate and subsequently exposed to a phosphor plate to quantify parent ^{18}F-mefway present in the blood. The phosphor plate was read by a Cyclone storage phosphor system (PerkinElmer) and analyzed with OptiQuant software. The plasma-free fraction (f_P) was measured with Centrifree ultrafiltration units (Millipore).

PET data were histogrammed into frames of 8 × 0.5, 3 × 2, 10 × 5, and 6 × 10 min. Sinogram data were then reconstructed with a filtered backprojection algorithm (Direct Inverse Fourier Transformation) using a 4-mm gaussian filter and included corrections for random events, deadtime, signal attenuation, and scanner normalization. Final images

jnm145151-pm ■ 10/24/14

had dimensions of 128 × 128 × 63, corresponding to voxel dimensions of 2.57 × 2.57 × 2.43 mm. Images of PET data summed from 1 to 10 min after injection, reflective of diffuse radioligand delivery throughout the brain, were used to register PET frames to the native space of the corresponding MR image using FSL's (Functional MRI of the Brain Software Library) Linear Image Registration Toolbox (*15*). The affine matrix was constrained to a rigid-body transformation (6 degrees of freedom.) because no intrasubject normalization was imposed.

Regions of interest were defined with FreeSurfer 5.3 software (http://surfer.nmr.mgh.harvard.edu). Regions extracted with this template-based algorithm included the amygdala, hippocampus, parahippocampal gyrus, insular cortex, anterior cingulate gyrus, posterior cingulate gyrus, parietal cortex, orbitofrontal cortex, temporal cortex, occipital [Fig. 2] cortex, and frontal cortex, shown in Figure 2. Additionally, the raphe nuclei region was manually drawn for each PET scan because this region's structure cannot be accurately determined using MR imaging data. To observe radioligand kinetic properties in regions of highest ^{18}F-mefway binding, PET data from a manually defined region of focal uptake in the MTL were also analyzed. This region included areas of the hippocampus proper, subiculum, dentate gyrus, and amygdala and was hand-drawn to minimize imperfect PET to MR imaging coregistration and partial-volume effects. Time–activity curves were extracted from all regions for subsequent analysis.

To compare measured cerebral radioactivity concentrations with other radioligands, the standardized uptake value (SUV) was calculated as SUV = PET/i.d. × mass × 1,000, where PET is the measured PET concentration (kBq/cm^3), i.d. is the injected dose (kBq), and mass is subject mass (kg). To quantify specific ^{18}F-mefway binding, binding potential based on nondisplaceable uptake (BP_{ND}) was measured. BP_{ND} is an index of receptor binding proportional to the product of receptor density (B_{max}) and radioligand–receptor affinity ($1/K_{Dapp}$) as $BP_{ND} = f_{ND}B_{max}/K_{Dapp}$, where f_{ND} is the free fraction of nondisplaceable radioligand in the tissue (*16*). Regional ^{18}F-mefway BP_{ND} values were calculated with the multilinear reference tissue model (MRTM) (*17*), assuming the cerebellum as a reference region. Logan graphical analysis (*18*) was used to calculate BP_{ND} values for comparison with the MRTM method and to visualize the establishment of radioligand psuedoequilbirum. Voxelwise ^{18}F-mefway BP_{ND} maps were also produced with Logan graphical analysis.

To assess the test–retest reproducibility of ^{18}F-mefway binding, early PET data from the retest scans (1–10 min after injection) were coregistered to the space of the test PET scan, allowing for 6 degrees of freedom. The affine matrix transforming the test PET data to the MR imaging was then applied to the retest PET data. Time–activity curves were extracted, and regional BP_{ND} values using MRTM were calculated as described above. The test–retest variability (TRV) between test and retest BP_{ND} values expressed as a percentage was calculated for each region with the relationship $TRV = Abs\{(BP_{ND(Test)} - BP_{ND(Retest)})/(BP_{ND(Test)} + BP_{ND(Retest)})/2\} \times 100$. Additionally, the intraclass correlation coefficient (ICC) (*19*) was calculated for each region.

RESULTS

Radiochemistry

^{18}F-mefway was produced with high yields greater than 1 GBq, with specific activities greater than 400 MBq/nmol. Radiochemical purity was 98.7% ± 2.8%, with chemical purities and stability greater than 90% at the time of expiration.

^{18}F-Mefway in Plasma

Venous blood samples were acquired to characterize the in vivo metabolism of ^{18}F-mefway. Acceptable radiochromatograms were acquired only for 4 subjects. Radio-TLC analysis of the plasma samples revealed the presence of radiolabeled metabolites as shown

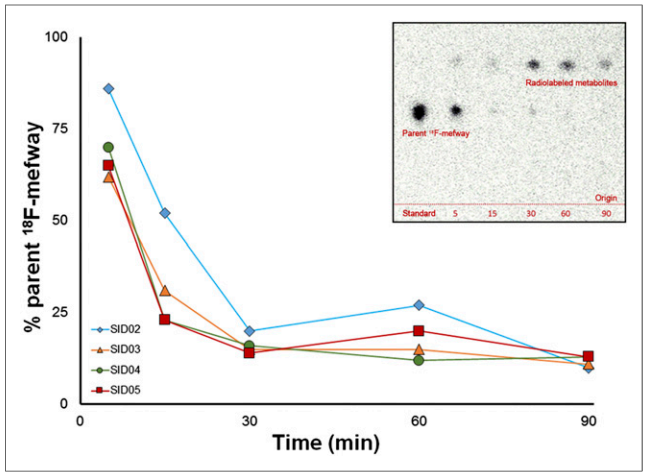

RGB

FIGURE 3. Metabolism of ^{18}F-mefway in vivo. Main plot shows percentage of total radioactivity in plasma attributed to parent ^{18}F-mefway. Each distinct color and shape corresponds to separate subject. Inset presents typical radiochromatogram. There is absence of detectable radioactivity at origin, expected location of ^{18}F-fluoride ion elution.

in Figure 3, although no attempt was made to assess any volatile [Fig. 3] species. The chemical nature of these metabolites was not characterized in the present work. Notably, no radiolabeled species were detectable at the origin of the chromatogram, suggesting negligible accumulation of ^{18}F-fluoride ions in the blood.

In vivo metabolism of ^{18}F-mefway was initially rapid, with parent compound accounting for less than 20% of total plasma radioactivity 30 min after injection. At this point, metabolism slowed, such that 10%–15% of the radioactivity in the plasma was ^{18}F-mefway at 90 min after injection (Fig. 3). The f_P of ^{18}F-mefway, measured for 5 of the 6 subjects, was 5.1% ± 0.7%.

^{18}F-Mefway Brain Uptake

Time–activity curves of ^{18}F-mefway uptake in the brain are [Fig. 4] illustrated in Figure 4. The time course of ^{18}F-mefway in the brain rapidly peaked at SUVs of roughly 1.7 after 1–2 min in the cerebellum and various cortical regions. Clearance of ^{18}F-mefway

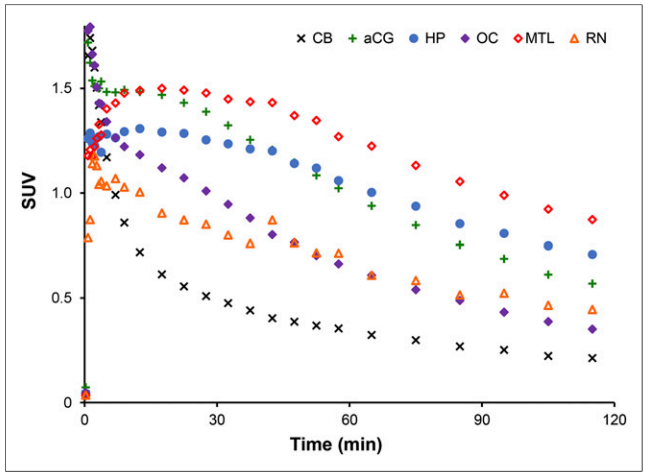

RGB

FIGURE 4. Representative ^{18}F-mefway time–activity curves. SUVs are defined as SUV = PET/i.d. × weight × 1,000. Regions shown include focal areas of uptake in MTL, hippocampus (HP), anterior cingulate gyrus (aCG), raphe nuclei (RN), occipital cortex (OC), and cerebellum (CB). i.d. = injected dose.

jnm145151-pm ■ 10/24/14

RGB

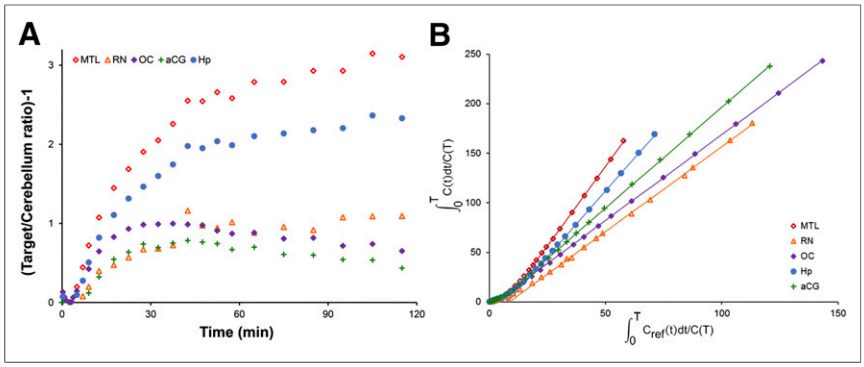

FIGURE 5. Kinetic properties of ^{18}F-mefway in vivo. (A) ^{18}F-mefway target-to-cerebellum ratios. (B) Logan plots, with t* = 45 min, to visualize pseudoequilibrium of tracer in various regions of brain. Regions shown include focal areas of uptake in MTL, hippocampus (Hp), anterior cingulate gyrus (aCG), raphe nuclei (RN), and occipital cortex (OC).

was rapid in the cerebellum, decreasing to half the peak value within 10 min after injection and approaching SUVs of 0.2 at 120 min after injection. In regions of high specific ^{18}F-mefway uptake, such as the MTL and hippocampus, peak uptake of ^{18}F-mefway was slower, plateauing within 15–20 min after injection with slow decreases in PET signal, reflective of specific ^{18}F-mefway [Fig. 5] binding. As illustrated in Figure 5A, ratios of ^{18}F-mefway concentrations in hippocampal regions relative to the cerebellum plateaued at roughly 60–90 min after injection at ratios ranging from 2 to 4.5. In cortical regions, these ratios plateaued faster with lower peak ratio values.

Specific ^{18}F-Mefway Binding

Estimates of BP_{ND} generated with MRTM2 for all regions examined are presented in Table 1. The highest values were observed [Table 1] in the MTL (2.42 ± 0.46). Estimates of BP_{ND} generated with the Logan reference region analysis method, using a linearization time t* = 45 min and omitting the $\overline{k_2}$ term, agreed within 3% of the estimates with MRTM. Sample Logan plots are illustrated in Figure 5B, showing the linearization of the data in all regions by 45 min after injection. A voxelwise BP_{ND} map, generated with Logan graphical analysis, is shown in Figure 6 [Fig. 6] for visualization of ^{18}F-mefway specific binding.

Retest ^{18}F-mefway scans were acquired for 5 subjects; however, 1 subject did not complete the scanning procedure, therefore only 4 retest scans were analyzed for test–retest analysis. For the 4 subjects with retest scans, the TRV averaged across all regions was 8% (Table 1). The ICC in regions of high ^{18}F-mefway uptake was greater than 0.88, indicating substantial agreement (*20*). Lower

TABLE 1
Scan Details and Regional ^{18}F-Mefway BP_{ND} Values with Test–Retest Analysis

Characteristic	Subject 1	2	3	4	5	6	Mean ± SD	TRV	ICC
Sex	F	F	M	M	F	F			
Age (y)	27	27	32	22	38	38	31 ± 7		
Weight (kg)	89	79	113	97	114	58	92 ± 21		
Injected activity (MBq)	204	192	200	204	196	196	199 ± 5		
Regional BP_{ND}*									
MTL†	2.59	2.23	3.15	1.86	2.63	2.07	2.42 ± 0.46	5.89	0.94
Hp	2.08	1.67	2.65	1.14	1.85	1.11	1.75 ± 0.59	3.69	0.99
Am	1.14	1.12	2.08	0.52	1.03	0.72	1.10 ± 0.54	11.55	0.99
pHp	1.74	1.65	2.24	1.27	1.80	1.10	1.63 ± 0.41	5.42	0.95
IC	1.61	1.53	2.19	1.27	1.40	1.52	1.59 ± 0.32	11.04	0.88
aCG	1.08	1.07	1.83	0.71	1.13	1.50	1.22 ± 0.39	8.94	0.98
pCG	0.86	0.73	1.54	0.51	0.85	0.87	0.89 ± 0.34	10.01	0.98
RN†	0.94	0.72	1.56	0.37	0.80	0.59	0.83 ± 0.41	11.35	0.97
PC	0.73	0.95	0.80	0.87	0.72	1.27	0.89 ± 0.20	10.06	0.60
OfC	1.08	0.88	1.68	0.85	1.02	1.31	1.14 ± 0.31	8.16	0.96
TC	1.27	1.39	1.31	1.27	1.20	1.51	1.32 ± 0.11	5.61	0.43
OC	0.63	0.75	0.79	0.64	0.66	0.89	0.73 ± 0.10	4.10	0.88
FC	0.77	0.99	0.81	0.79	0.73	1.37	0.91 ± 0.24	9.04	0.71

*BP_{ND} values calculated with MRTM.
†Denotes PET-defined regions.
Regions included are focal areas of uptake in MTL (hand-drawn), hippocampus (Hp), amygdala (Am), parahippocampal gyrus (pHp), insular cortex (IC), anterior cingulate gyrus (aCG), posterior cingulate gyrus (pCG), parietal cortex (PC), orbitofrontal cortex (OfC), temporal cortex (TC), occipital cortex (OC), frontal cortex (FC), and raphe nuclei (RN; PET-defined).

jnm145151-pm ■ 10/24/14

RGB

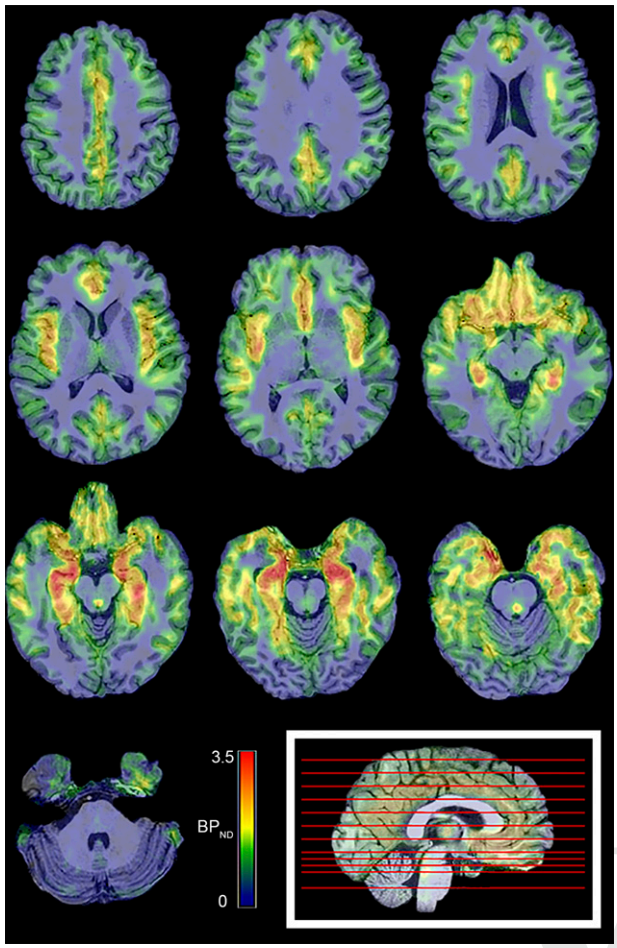

FIGURE 6. Voxel-wise ^{18}F-mefway BP_{ND} maps overlaid on coregistered MR image. Parametric BP_{ND} images are linearly scaled from 0 to 3.5. Location of each transverse slice is denoted by red lines on midsagittal slice at bottom right.

values were measured in areas of moderate uptake, likely due to the reduced BP_{ND} values in these regions.

DISCUSSION

This study demonstrates that ^{18}F-mefway has favorable specific binding levels and kinetic properties for human PET imaging of 5-HT_{1A} receptors. Reliable imaging of the 5-HT_{1A} system has been an important goal of the neuroimaging community, yet lack of a suitable radioligand has stunted successful widespread PET imaging of 5-HT_{1A} receptors due to limitations in areas such as radiochemistry, quantitation, defluorination, and brain penetration. ^{18}F-mefway possesses a simple radiochemical production, brain uptake levels comparable to other 5-HT_{1A} radioligands, a high signal-to-noise ratio, suitable kinetic properties, no apparent PET signal in bone, and higher detected nonspecific PET signal than ^{11}C radioligands, making it a promising candidate for imaging 5-HT_{1A} receptors in humans.

Radio-TLC techniques were used to measure the rate of ^{18}F-mefway metabolism in vivo. The results indicated initial rapid metabolism of ^{18}F-mefway, followed by a slow metabolism component such that 10%–15% of the radioactivity in the plasma was attributed to parent ^{18}F-mefway after 90 min in the blood. Low counting statistics in the blood samples at late times due to rapid metabolism and low f_P limited the precision of these measurements. The rate of ^{18}F-mefway metabolism was slightly slower than ^{11}C-WAY-100635 and ^{18}F-FCWAY (*21*, *22*).

The in vivo metabolism of ^{11}C-WAY-100635 and ^{18}F-FCWAY results in radiolabeled cyclohexanecarboxylic acid species, both of which crossed the blood–brain barrier (*21,22*). A similar potential metabolite species of ^{18}F-mefway, ^{18}F-*trans*-4-fluoromethylcyclohexanoic acid, showed little to no brain penetration in rat PET studies (*23*). We have not fully characterized the metabolite species of ^{18}F-mefway in humans for the present work; thus, the potential for ^{18}F-*trans*-4-fluoromethylcyclohexanoic acid accumulation in the human brain remains a matter for future studies. The f_P of ^{18}F-mefway was measured at 5.1%, with little variability between subjects. This low free fraction is consistent with the values of other radioligands specific to 5-HT_{1A} receptors.

Specific uptake of ^{18}F-mefway in the human brain was consistent with the cerebral distribution of 5-HT_{1A} receptors (*24*). The highest measured ^{18}F-mefway BP_{ND} levels were 2.4 in the regions in the MTL, with values of 1.6 in the insular cortex, 1.2 in the anterior cingulate gyrus, 0.8 in the raphe nuclei, and 0.6–0.9 in the occipital cortex. These human ^{18}F-mefway BP_{ND} values are roughly 3–4 times lower than reported ^{11}C-WAY-100635 BP_{ND} values derived using an atlas-based approach (*25*). However, a direct comparison of these radioligands in human subjects with the same scanners and data processing techniques will be needed to identify in vivo differences between radiotracers. Such studies previously performed in nonhuman primates demonstrated comparable levels of BP_{ND} between ^{18}F-mefway and ^{11}C-WAY-100635 (*11*). Although interspecies differences may explain some of the variation in ^{18}F-mefway binding between humans and monkeys, the atlas-based ROI definition in this work likely reduced BP_{ND} because of spatial averaging, compared with the manual ROI definition in our previous work.

The behavior of 5-HT_{1A}–specific radioligands in the cerebellum is a crucial issue for accurate assay of 5-HT_{1A} binding. Use of the cerebellum with reference region analysis strategies can avoid the need for arterial blood sampling. The cerebellum has been used as a reference region for quantitation of BP_{ND} with 5-HT_{1A} radioligands because of minimal specific binding levels (*26*). Small levels of specific ^{11}C-WAY-100635 binding were subsequently observed in the cerebellar gray matter and vermis (*27*), indicating a potential underestimation in BP_{ND} with cerebellar gray matter. White matter regions have been proposed as potential reference regions to avoid this bias of BP_{ND} estimates (*28,29*), which assumes similar nonspecific radioligand behavior in both white matter and gray matter. We speculate that the strategies developed to account for potential binding of other 5-HT_{1A} radioligands in the cerebellum will be applicable to ^{18}F-mefway procedures as well. Further investigation is needed to fully characterize potential specific binding in the cerebellum and its ramifications on the analysis of ^{18}F-mefway PET data.

The time course of ^{18}F-mefway in the cerebellum was characterized by rapid washout, followed by low radioactivity concentrations (Fig. 4). These cerebellar characteristics are similar for other 5-HT_{1A} radioligands, resulting in low counting statistics in the cerebellum at late times. Such regions are subject to bias depending on the scatter correction and reconstruction algorithms used in processing the PET data (*30*) and subsequently bias BP_{ND} estimates when used as reference regions. Given the similar cerebellar SUVs of ^{18}F-mefway and ^{11}C-WAY-10036 (*31*) at 90 min, the 110-min

jnm145151-pm ■ 10/24/14

RGB

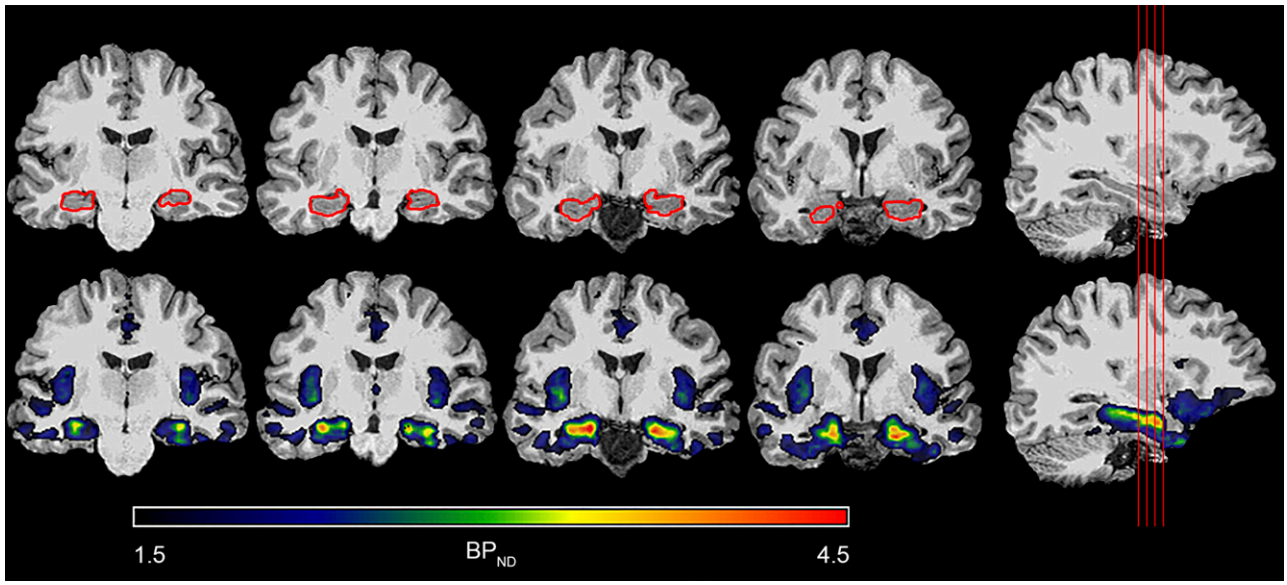

FIGURE 7. Delineation of specific ^{18}F-mefway binding in MTL. (Top) T1-weighted MR image with corresponding hippocampal FreeSurfer mask drawn in red. (Bottom) ^{18}F-mefway BP_{ND} parametric image overlaid on same MR image. BP_{ND} linear thresholding ranges from 1.5 to 4.5. Red lines on far right sagittal slice indicate location of corresponding coronal slices.

half-life of the ^{18}F isotope, compared with the 20-min half-life of ^{11}C, yields more than 12-fold more real measured counts by the PET scanner. This characteristic, and the opportunity to conduct PET studies with an off-site cyclotron, are important practical advantages of ^{18}F-labeled 5-HT_{1A} radioligands. One potential cause of low cerebellar uptake for 5-HT_{1A}–specific radioligands is the P-glycoprotein transporter, as demonstrated for ^{18}F-MPPF (*32,33*). The potential regulation of ^{18}F-mefway brain penetration by P-glycoprotein is an important question for future investigation.

Previous ^{18}F-FCWAY studies exhibited bone uptake of ^{18}F-fluoride ions, resulting in the spill-in of detected PET signal from the surrounding skull into the cerebellum and subsequently requiring the use of enzyme inhibitors for accurate ^{18}F-FCWAY quantification (*7,8*). Low levels of PET signal in bone were evident in rat ^{18}F-mefway studies (*34*) but not in rhesus monkeys (*11*). The present data were closely inspected for potential bone uptake of radiolabeled species in human subjects. The PET images did not indicate any areas of elevated ^{18}F-mefway uptake in regions immediately surrounding the brain. Cerebellar time–activity curves decreased at late times, instead of plateauing or increasing (which would reflect the spill-in of PET signal from surrounding bone). Furthermore, the radio-TLC analysis did not reveal a detectable signal at the expected location of ^{18}F-fluoride ion elution (the origin; Fig. 3A). These studies provide evidence for negligible accumulation of radiolabeled species in bone; however, they are not conclusive. Future planned PET/CT studies, providing accurate localization of the skull, will conclusively determine the reported absence of bone uptake.

Typical ^{11}C-WAY-100635 scans require 90 min for accurate quantification. Although 120 min of ^{18}F-mefway data were acquired for the present scans, the data were truncated at 90 min and BP_{ND} values were recalculated with MRTM. Calculated BP_{ND} from the 90-min truncated dataset agreed well with BP_{ND} from the full dataset, with an R^2 of 0.99. There was a slight negative bias due to a systematic BP_{ND} underestimation of 3% in the MTL regions of highest ^{18}F-mefway binding. This small bias in regions of extreme ^{18}F-mefway binding may be acceptable in exchange for reduced duration of scanning procedures. Therefore, it is likely that 90 min will be an appropriate scanning time for accurate quantification of ^{18}F-mefway binding.

Values of ^{18}F-mefway TRV averaged 8% across all regions, indicating good agreement in repeated scans. The ICC values were strong in regions of high ^{18}F-mefway binding. Reduced ICC values were observed in regions of lower ^{18}F-mefway specific binding, likely due to lower BP_{ND} values in these regions. The test–retest properties of ^{18}F-mefway are encouraging for future human PET studies implementing a 2-scan experimental design.

The binding profile of ^{18}F-mefway allowed for close inspection of the regional distribution of specific binding in the MTL, as visualized in Figure 7. The region of highest ^{18}F-mefway binding [**Fig. 7**] was the hippocampus. Relatively lower binding levels were observed in the subiculum sublayer, located more medially than CA1–CA4, and the amygdala. Less ^{18}F-mefway binding was also evident in the parahippocampal gyrus and the most posterior regions of the hippocampus near the crux of the fornix. These differences in specific ^{18}F-mefway uptake yielded exquisite delineation of 5-HT_{1A} binding in the MTL. Consequently, ^{18}F-mefway PET data from this region, most prominently in the hippocampus, may have clinical utility in studying both healthy pathology and neurologic and psychiatric disorders that affect the MTL.

CONCLUSION

These initial studies of ^{18}F-mefway in humans prove highly promising. The simple radiochemical production, high specific radioligand uptake, ^{18}F radiolabel, and lack of PET signal in bone make ^{18}F-mefway a promising candidate for assay of 5-HT_{1A} receptors with human PET. Future studies to assess the viability of ^{18}F-mefway in pathology-specific populations are merited.

jnm145151-pm ■ 10/24/14

DISCLOSURE

The costs of publication of this article were defrayed in part by the payment of page charges. Therefore, and solely to indicate this fact, this article is hereby marked "advertisement" in accordance with 18 USC section 1734. Support for this research was provided by R33AG030524, T32CA009206, and P30HD03352. No other potential conflict of interest relevant to this article was reported.

ACKNOWLEDGMENTS

We thank R. Jerry Nickles and Hector Valdovinos for assistance with radioisotope production, Dr. Dhanabalan Murali for assistance with radiochemical production of ^{18}F-mefway, and Dr. Steve Kecskemeti for assistance with MRI data acquisition and processing. Sharon Kuruvilla provided important assistance with figure preparation. We are grateful to Barb Mueller and Travis Doran for their contributions with scanning procedures and to the volunteer subjects for their participation in this study.

REFERENCES

1. Blier P, Ward NM. Is there a role for 5-HT$_{1A}$ agonists in the treatment of depression? *Biol Psychiatry.* 2003;53:193–203.
2. Raymond JR, Mukhin YV, Gettys TW, Garnovskaya MN. The recombinant 5-HT$_{1A}$ receptor: G protein coupling and signaling pathways. *Br J Pharmacol.* 1999;127:1751–1764.
3. Pike VW, McCarron JA, Lammertsma AA, et al. Exquisite delineation of 5-HT$_{1A}$ receptors in human brain with PET and ^{11}C-WAY-100635. *Eur J Pharmacol.* 1996;301:R5–R7.
4. Kumar JSD, Mann JJ. PET tracers for 5-HT$_{1A}$ receptors and uses thereof. *Drug Discov Today.* 2007;12:748–756.
5. Aznavour N, Zimmer L. ^{18}F-MPPF as a tool for the in vivo imaging of 5-HT$_{1A}$ receptors in animal and human brain. *Neuropharmacology.* 2007;52:695–707.
6. Carson RE, Lang L, Watabe H, et al. PET evaluation of ^{18}F-FCWAY, an analog of the 5-HT$_{1A}$ receptor antagonist, WAY-100635. *Nucl Med Biol.* 2000;27:493–497.
7. Carson RE, Wu Y, Lang L, et al. Brain uptake of the acid metabolites of ^{18}F-labeled WAY 100635 analogs. *J Cereb Blood Flow Metab.* 2003;23:249–260.
8. Tipre DN, Zoghbi SS, Liow JS, et al. PET imaging of brain 5-HT$_{1A}$ receptors in rat in vivo with ^{18}F-FCWAY and improvement by successful inhibition of radioligand defluorination with miconazole. *J Nucl Med.* 2006;47:345–353.
9. Wooten D, Hillmer AT, Murali D, et al. An in vivo comparison of *cis*- and *trans*-^{18}F-mefway in the nonhuman primate. *Nucl Med Biol.* 2011;38:925–932.
10. Saigal N, Pichika R, Easwaramoorthy B, et al. Synthesis and biologic evaluation of a novel serotonin 5-HT$_{1A}$ receptor radioligand, ^{18}F-labeled mefway, in rodents and imaging by PET in a nonhuman primate. *J Nucl Med.* 2006;47:1697–1706.
11. Wooten DW, Moraino JD, Hillmer AT, et al. In vivo kinetics of ^{18}F-mefway: a comparison with ^{11}C-WAY100635 and ^{18}F-MPPF in the nonhuman primate. *Synapse.* 2011;65:592–600.
12. Wooten DW, Hillmer AT, Moirano JM, et al. 5-HT$_{1A}$ sex based differences in B_{max}, in vivo K_D, and BP_{ND} in the nonhuman primate. *Neuroimage.* 2013;77:125–132.
13. Christian BT, Wooten DW, Hillmer AT, et al. Serotonin transporter genotype affects serotonin 5-HT$_{1A}$ binding in primates. *J Neurosci.* 2013;33:2512–2516.
14. Hillmer AT, Wooten DW, Tudorascu D, et al. The effects of chronic alcohol self-administration on serotonin 5-HT$_{1A}$ binding in nonhuman primates. *Drug Alcohol Depend.* August 29, 2014 [Epub ahead of print].
15. Jenkinson M, Bannister P, Brady M, Smith S. Improved optimization for the robust and accurate linear registration and motion correction of brain images. *Neuroimage.* 2002;17:825–841.
16. Innis RB, Cunningham VJ, Delforge J, et al. Consensus nomenclature for in vivo imaging of reversibly binding radioligands. *J Cereb Blood Flow Metab.* 2007;27:1533–1539.
17. Ichise M, Liow J-S, Lu J-Q, et al. Linearized reference tissue parametric imaging methods: application to ^{11}C-DASB positron emission tomography studies of the serotonin transporter in human brain. *J Cereb Blood Flow Metab.* 2003;23:1096–1112.
18. Logan J, Fowler JS, Volkow ND, Wang GJ, Ding YS, Alexoff DL. Distribution volume ratios without blood sampling from graphical analysis of PET data. *J Cereb Blood Flow Metab.* 1996;16:834–840.
19. Shrout PE, Fleiss JL. Intraclass correlations: uses in assessing rater reliability. *Psychol Bull.* 1979;86:420–428.
20. Shrout PE. Measurement reliability and agreement in psychiatry. *Stat Methods Med Res.* 1998;7:301–317.
21. Osman S, Lundkvist C, Pike VW, et al. Characterisation of the appearance of radioactive metabolites in monkey and human plasma from the 5-HT$_{1A}$ receptor radioligand, carbonyl-^{11}C-WAY-100635: explanation of high signal contrast in PET and an aid to biomathematical modelling. *Nucl Med Biol.* 1998;25:215–223.
22. Ma Y, Kiesewetter DO, Lang L, et al. Determination of ^{18}F-FCWAY, ^{18}F-FP-TZTP, and their metabolites in plasma using rapid and efficient liquid-liquid and solid phase extractions. *Nucl Med Biol.* 2003;30:233–240.
23. Saigal N, Bajwa AK, Faheem SS, et al. Evaluation of serotonin 5-HT$_{1A}$ receptors in rodent models using ^{18}F-mefway PET. *Synapse.* 2013;67:596–608.
24. Hall H, Lundkvist C, Halldin C, et al. Autoradiographic localization of 5-HT$_{1A}$ receptors in the post-mortem human brain using ^{3}H-WAY-100635 and ^{11}C-WAY-100635. *Brain Res.* 1997;745:96–108.
25. Rabiner EA, Messa C, Sargent PA, et al. A database of ^{11}C-WAY-100635 binding to 5-HT$_{1A}$ receptors in normal male volunteers: normative data and relationship to methodological, demographic, physiological, and behavioral variables. *Neuroimage.* 2002;15:620–632.
26. Gunn RN, Sargent PA, Bench CJ, et al. Tracer kinetic modeling of the 5-HT$_{1A}$ receptor ligand carbonyl-^{11}C-WAY-100635 for PET. *Neuroimage.* 1998;8:426–440.
27. Parsey RV, Arango V, Olvet DM, Oquendo MA, Van Heertum RL, Mann JJ. Regional heterogeneity of 5-HT$_{1A}$ receptors in human cerebellum as assessed by positron emission tomography. *J Cereb Blood Flow Metab.* 2005;25:785–793.
28. Hirvonen J, Kajander J, Allonen T, Oikonen V, Någren K, Hietala J. Measurement of serotonin 5-HT$_{1A}$ receptor binding using positron emission tomography and carbonyl-^{11}C-WAY-100635-considerations on the validity of cerebellum as a reference region. *J Cereb Blood Flow Metab.* 2007;27:185–195.
29. Giovacchini G, Conant S, Herscovitch P, Theodore WH. Using cerebral white matter for estimation of nondisplaceable binding of 5-HT$_{1A}$ receptors in temporal lobe epilepsy. *J Nucl Med.* 2009;50:1794–1800.
30. Bélanger MJ, Mann JJ, Parsey RV. OS-EM and FBP reconstructions at low count rates: effect on 3D PET studies of ^{11}C-WAY-100635. *Neuroimage.* 2004;21:244–250.
31. Parsey RV, Slifstein M, Hwan D-R, et al. Validation and reproducibility of measurement of 5-HT$_{1A}$ receptor parameters with [*carbonyl*-^{11}C]WAY-100635 in humans: comparison of arterial and reference tissue input functions. *J Cereb Blood Flow Metab.* 2000;20:1111–1133.
32. Passchier J, van Waarde A, Doze P, Elsinga PH, Vaalburg W. Influence of P-glycoprotein on brain uptake of ^{18}F-MPPF in rats. *Eur J Pharmacol.* 2000;407:273–280.
33. Tournier N, Cisternino S, Peyronneau MA, et al. Discrepancies in the P-glycoprotein-mediated transport of ^{18}F-MPPF: a pharmacokinetic study in mice and non-human primates. *Pharm Res.* 2012;29:2468–2476.
34. Choi JY, Kim CH, Jeon TJ, et al. Effective microPET imaging of brain 5-HT$_{1A}$ receptors in rats with ^{18}F-mefway by suppression of radioligand defluorination. *Synapse.* 2012;66:1015–1023.